JOURNAL OF CATALYSIS 149, 211–222 (1994)

Platinum–Mordenite Catalysts for *n*-Hexane Isomerization: Characterization by X-Ray Absorption Spectroscopy and Chemical Probes

Mark M. Otten, Matthew J. Clayton, and H. Henry Lamb[1]

Department of Chemical Engineering, North Carolina State University, Box 7905, Raleigh, North Carolina 27695-7905

Received January 3, 1994; revised May 4, 1994

Platinum–mordenite (Pt–MOR) catalysts were prepared from NH_4–MOR by ion exchange with $[Pt^{II}(NH_3)_4][OH]_2$, calcination in O_2 at 350°C, and reduction in H_2 at 350°C. The resultant Pt–H–MOR was active for *n*-hexane isomerization and hydrocracking via bifunctional catalysis at 240–300°C and 1 atm. The observed activation energies for C_6 branched-isomer formation are unusually low, suggesting that the isomerization rates were controlled by pore diffusion. A Pt–KH–MOR catalyst was prepared by ion exchange with aqueous KNO_3 and re-reduction at 350°C; elemental analysis evidenced 90% exchange of protons for K^+ ions. The product distribution and observed activation energies for C_6 branched-isomer formation over Pt–KH–MOR are consistent with *n*-hexane isomerization via bifunctional catalysis. Hydrocracking was strongly suppressed, and light hydrocarbons were formed primarily by Pt-catalyzed hydrogenolysis. From *in situ* extended X-ray absorption fine structure spectroscopy and H_2 temperature-programmed desorption, we conclude that the Pt–MOR catalysts consist of small Pt clusters hosted within the mordenite crystals. The Pt L_{III} X-ray absorption near-edge structure (XANES) spectra of Pt–H–MOR and Pt–KH–MOR are closely similar, suggesting that the electronic structure of the Pt clusters is unaffected by mordenite acid–base chemistry. For the freshly reduced catalysts, a XANES feature at 10 eV relative energy is assigned to Pt–H antibonding states. The infrared spectrum of CO adsorbed on Pt–H–MOR contains an intense band at 2084 cm^{-1}, which is assigned to linear CO moieties on Pt clusters. A small peak at 2124 cm^{-1} is assigned to isolated Pt^I–CO species, which we infer are formed by oxidative fragmentation of Pt clusters. The infrared spectrum of CO adsorbed on Pt–KH–MOR evidences a red shift of the linear CO band, which we suggest is due to electrostatic interactions between carbonyl O atoms and nearby K^+ ions. © 1994 Academic Press, Inc.

INTRODUCTION

Support acidity can markedly influence the product distribution of *n*-hexane conversion over Pt–zeolite catalysts. Pt–K–L and Pt–BaK–L catalysts are highly selective for the aromatization of *n*-hexane to benzene (1). The high aromatization selectivity of Pt clusters hosted in L zeolite was ascribed first to a geometrical influence of the zeolite channels (2), but recent studies indicate that the extremely small size of the Pt clusters and the absence of support acidity are responsible (3, 4). Platinum–hydrogen–mordenite (Pt–H–MOR) catalysts are used commercially for isomerization of C_5–C_6 normal alkanes to higher-octane branched isomers (5). Isomerization is believed to occur via bifunctional catalysis (6), involving both acid and metal sites. Yield loss from formation of light alkane products can occur by bifunctional hydrocracking and by monofunctional Pt-catalyzed hydrogenolysis (7, 8).

Typically, highly dispersed Pt–zeolite catalysts are prepared by ion exchange (e.g., with tetraamine Pt^{II}). Calcination by slow heating in flowing O_2 to 300–350°C and subsequent reduction in H_2 are reported to produce intracrystalline Pt clusters (9, 10). The low Pt loadings of Pt–H–MOR catalysts (typically 0.3–1% by weight) and the large internal surface area of the support favor formation of Pt clusters containing only a few atoms. In this regime, size and support effects on Pt electronic structure have been reported (11). Small Pt clusters in zeolites have been characterized as electron deficient on the basis of data from X-ray photoelectron spectroscopy (XPS) (12, 13), infrared spectroscopy of adsorbed CO (14), and X-ray absorption near-edge structure (XANES) spectroscopy (15). Electron deficiency is believed to be greatest for Pt clusters in hydrogen zeolites. Recently, Samant and Boudart reported the characterization of Pt clusters containing 20–40 atoms in Y zeolite using extended X-ray absorption fine structure (EXAFS) spectroscopy, XANES spectroscopy, chemisorption measurements, and Fourier transform infrared (FTIR) spectroscopy of adsorbed CO (16). They concluded that there was no evidence of charge transfer from the Pt to the support and that the intrazeolitic Pt clusters were electron deficient owing to their small size. Nonetheless, Samant and Boudart inferred from FTIR spectra of adsorbed CO and

[1] To whom correspondence should be addressed.

0021-9517/94 $6.00

chemisorption measurements that the ionization potential of Pt increases with support acidity.

Herein, we report the preparation, testing, and characterization of Pt–MOR catalysts for *n*-hexane isomerization. To suppress hydrocracking activity, Pt–H–MOR catalysts were reduced and then most of the protons were exchanged for K^+ ions. The Pt–H–MOR and Pt–KH–MOR catalysts were characterized by EXAFS, XANES, and FTIR spectroscopies and by temperature-programmed desorption of H_2 (H_2 TPD) to determine the Pt cluster size and the effects of mordenite acidity on Pt electronic structure.

EXPERIMENTAL METHODS

Catalyst preparation. Dealuminated Na–MOR (Tosoh, SiO_2/Al_2O_3 = 18.5) with an average crystallite size of 0.5 μm was ion-exchanged three times with 2 *M* NH_4NO_3 solution at 32°C. The resultant NH_4–MOR was washed with 18-MΩ deionized (DI) water and dried in air at 100°C. A 1000-ppm solution of $[Pt(NH_3)_4][OH]_2$ (Strem Chemicals) in DI water (40 ml) was added dropwise to a slurry of NH_4–MOR (4 g) in DI water (40 ml). The initial 1000-ppm $[Pt(NH_3)_4][OH]_2$ solution was basic (pH 11); after exchange, the solution was nearly neutral (pH 7.3–7.5). After a contact time of at least 12 h, the Pt-exchanged mordenite was recovered by filtration, washed with DI water, and dried in air at 100°C. Pt(II)–NH_4–MOR (2 g) was heated at 0.5°C/min to 350°C in flowing extra-dry O_2 (600–700 ml/min) and held at this temperature for 2–3 h. The resultant Pt(II)–H–MOR was yellow-green after the O_2 treatment, but turned pale green during transfer in air. Pt–KH–MOR catalysts were prepared by twice exchanging Pt–H–MOR samples, which had been reduced in H_2 at 350°C, with a 40% excess (estimated from the Si/Al ratio) of KNO_3 in aqueous solution. Each sample was washed with DI water and dried at 100°C after K^+ exchange. The catalysts were stored in a desiccator until needed.

n-Hexane isomerization and cracking. Catalyst samples (0.30 g) were supported on plugs of glass wool in Pyrex reactor tubes. The catalysts were dried in flowing He (20 liters/h/g) for 1 h at 200°C, cooled to below 50°C, and reduced in a stream of flowing H_2 (20 liters/h/g) by heating at 5°C/min to 350°C and holding at this temperature for 1 h. The catalysts were allowed to cool to 300°C in flowing H_2 and then tested for *n*-hexane conversion. The reactant stream was generated by passing H_2 (100 ml/min) through a saturator containing *n*-hexane (Fisher, 99%) at 25°C. GC analysis indicated that the hydrogen/*n*-hexane mixture was within 10% of saturation at 25°C, corresponding to a H_2 : HC mole ratio of 4.0. The reactor effluent was analyzed for C_1–C_6 hydrocarbons by gas chromatography at 70°C using a 30-ft, ⅛-in. stainless-steel column containing 23% SP-1700 on 80/100 Chromosorb P AW (Supelco). The *n*-hexane was contaminated by small amounts of 3-methylpentane and methylcyclopentane; this was taken into consideration in the data analysis. All tubing between the *n*-hexane source and the gas chromatograph was heat-traced to prevent condensation. The catalysts typically deactivated approximately 5% during the first hour on stream, and deactivated more slowly after that (<5% in 5 h). After a catalyst had been on stream for 1.5 h at 300°C, the temperature dependence of the reaction rates was determined by taking measurements between 240 and 300°C. After the temperature was changed, the reactor required about 1 h to achieve steady state. Typically, the reported production rates at each temperature are averages of four measurements taken over a 3-h period.

X-ray absorption spectroscopy. X-ray absorption spectroscopy (XAS) measurements were made on beamline X-11A at the National Synchrotron Light Source, Brookhaven National Laboratory. The storage-ring energy was 2.5 GeV and the current decayed from 250 to 110 mA during a typical fill. The beamline monochromator was equipped with a pair of Si(111) crystals for operation in the region of the Pt L_{III} absorption edge. Transmission spectra were recorded by using gas-filled ionization chambers to measure the incident (I_0) and transmitted (I) beams. Reference spectra were recorded simultaneously by placing a thin Pt foil between the I detector and a third ionization chamber (I_{ref}). Normalized EXAFS and XANES spectra were obtained from the experimental XAS data by using standard data processing procedures (17). The EXAFS data were Fourier-filtered to isolate the first coordination shell, and the resultant chi function was fitted in k space using a reference derived from the EXAFS spectrum of Pt foil at approximately −196°C.

Calcined [Pt(II)–H–MOR] and K^+-exchanged (Pt–KH–MOR) samples were loaded in high-vacuum-compatible XAS cells and treated at the beamline. Samples were evacuated at 150°C for 0.5 h, cooled to below 50°C, and reduced in flowing H_2 (100 ml/min) at 350°C for 1 h. Spectra were measured with the samples under H_2 and cooled to approximately −173°C. After the initial XAS measurement, a Pt–H–MOR sample was evacuated (to base pressure of 10^{-6} Torr) at 300°C for 0.5 h; the cell was back-filled with He and the XAS spectrum measured at approximately −173°C. Another Pt–H–MOR sample was heated in static H_2 to 300°C and then exposed to H_2 (100 ml/min) saturated with *n*-hexane. After 1 h under reaction conditions, the catalyst was cooled in flowing H_2, and its XAS spectrum was measured, as described above. H_2 and He (UHP grade) were used after passage through water- and oxygen-getter traps.

H_2 TPD. Catalyst samples (0.4 g) were loaded into a fritted quartz tube and dried in flowing He (100 ml/min)

TABLE 1

Elemental Composition of Pt–MOR Catalysts[a]

Catalyst	Element					
	Si (wt%)	Al (wt%)	K (wt%)	Pt (wt%)	Na (ppm)	Fe (ppm)
Pt–H–MOR	39.13	4.23	—	0.89	12	321
Pt–KH–MOR	33.40	3.39	4.35	0.84	—	—

[a] Performed by Galbraith Laboratories, Inc. A dash indicates that an analysis was not performed for that element.

for 1 h at 200°C. The samples were cooled to less than 50°C, and the gas stream was switched to H_2. Samples were reduced in flowing H_2 (100 ml/min) at 350°C for 1 h and cooled to below 30°C. The gas stream was switched to Ar, and the reactor was purged until a constant baseline was observed on a downstream thermal conductivity detector (TDC). The sample was then heated at 10°C/min to 600° C, and the thermal conductivity difference between the Ar streams (5 ml/min) entering and exiting the reactor was recorded. A liquid-N_2/acetone slush bath, which was located between the reactor and the working side of the TDC, was used to trap condensable gases.

FTIR spectroscopy. Self-supporting wafers (approximately 50 mg each) of Pt(II)–H–MOR and Pt–KH–MOR were pressed using a circular die. Wafers were pretreated and measured in glass cells which were fitted with NaCl windows and high-vacuum stopcocks. Before CO adsorption, samples were pretreated by evacuation at 150°C for 0.5 h, reduction in flowing H_2 at 350°C for 1 h, and evacuation at 300°C for 0.5 h (to base pressure of 10^{-6} Torr); the samples were allowed to cool to less than 50°C after each pretreatment step. At 30°C, samples were exposed to CO at 100 Torr for 15 min. FTIR spectra were recorded after CO desorption for 15 min *in vacuo* at 30, 100, and 200°C. Each spectrum was recorded at 30°C. To obtain the presented spectra, zeolite absorption bands in the region of interest were removed by subtraction.

RESULTS AND DISCUSSION

1. Catalysis of n-Hexane Isomerization and Cracking

Pt–H–MOR Catalysts. The elemental composition of the Pt(II)–H–MOR catalyst after calcination at 350°C in flowing O_2 is given in Table 1. This corresponds to a unit cell formula of $H_{4.6}Pt_{0.14}Al_{4.9}Si_{43.1}O_{96}$, which is in good agreement with the reported Si/Al ratio of 9.2. The Pt loading corresponds to about 1 Pt atom per 7 unit cells or equivalently 1 Pt per 120 Å of mordenite channel length. The catalyst contained a negligible amount of residual Na. The Fe content, although in the range expected for a good commercial material, is a concern, as it corresponds to about 1 Fe atom per 10 Pt atoms. Catalysts were tested for *n*-hexane conversion following *in situ* reduction in flowing H_2 at 350°C.

At 300°C and 1 atm (H_2:HC = 4), the yield of C_6 branched isomers from *n*-hexane is nearly 75% over Pt–H–MOR. The balance of the products consists almost exclusively of light alkanes; the methylcyclopentane (mcp) yield is less than 1%. The detailed product distribution is given in Table 2. The C_6 branched alkane isomers are those expected for *n*-hexane isomerization via bifunctional catalysis (Scheme I) (18). The metal function serves to establish equilibrium between alkanes and alkenes, and the acid sites protonate the alkenes to form carbenium ions. The resultant secondary carbenium ions isomerize to form more stable tertiary carbenium ions, but also undergo oligomerization and β-scission. The tertiary carbenium ions form branched alkenes and alkanes via proton transfer or hydride abstraction reactions, respectively. Cracking via β-scission of teritary hexyl carbenium ions is expected to be prohibitively slow, owing to the very low stabilities of the resultant primary and methyl carbenium ions.

For bifunctional catalysts with sufficient metal sites, skeletal rearrangement of secondary carbenium ions is believed to be the rate-limiting step in isomerization (6b).

TABLE 2

Conversions and Product Distributions for *n*-Hexane Reaction over Pt–MOR Catalysts at 300°C and 1 atm

% Conversion: Product	Catalyst	
	Pt–H–MOR 7	Pt–KH–MOR 4
	% Yield[a]	
Methane	0.23	0.55
Ethane	0.69	1.0
Propane	9.0	2.1
Isobutane	6.9	0.18
n-Butane	2.4	1.8
Isopentane	4.6	0.30
n-Pentane	2.1	2.0
$\Sigma(C_1$–$C_5)$	25.9	7.9
2,3-dmb	3.9	0.90
2-mp	48.1	55.4
3-mp	21.2	32.1
$\Sigma(i$-$C_6)$	73.2	88.4
mcp	0.93	3.8
benzene	—	trace

[a] Moles of *n*-hexane converted to each product per 100 total moles of *n*-hexane consumed.

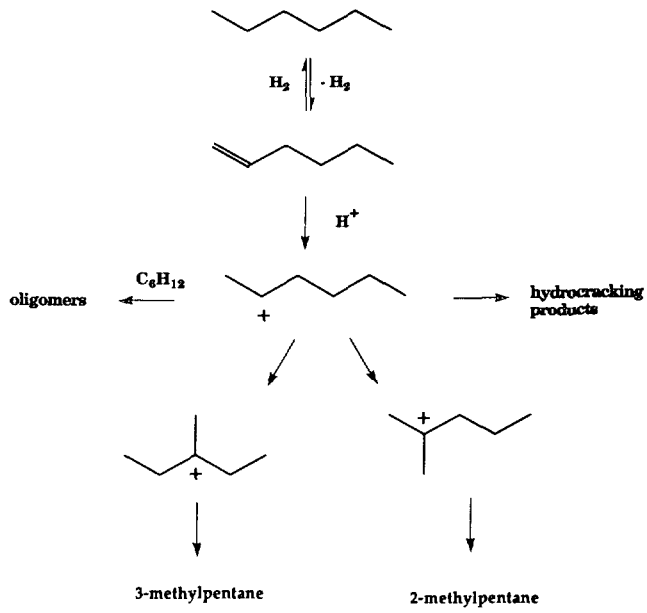

SCHEME I

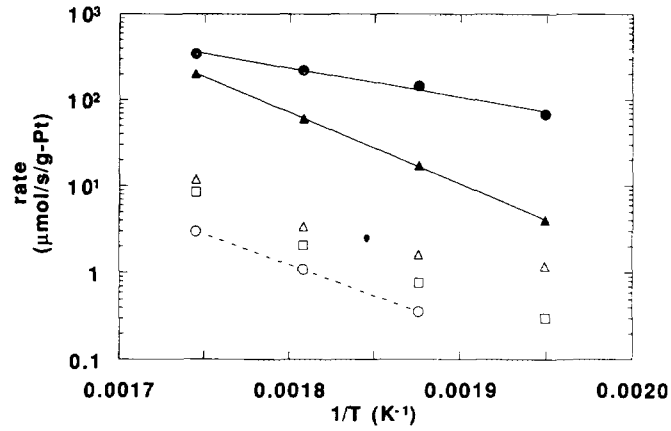

FIG. 1. Arrhenius plot for *n*-hexane conversion over Pt–H–MOR: $\Sigma(i\text{-}C_6)$ (solid circles), $\Sigma(C_1\text{–}C_3)$ (solid triangles), ethane (open triangles), methane (open squares), methylcyclopentane (open circles). Reaction conditions: P = 1 atm, H_2:HC = 4.0 (molar basis).

Methylpentanes (2-mp and 3-mp) and 2,3-dimethylbutane (2,3-dmb) are reported to be primary products of *n*-hexane isomerization over Pt–H–MOR catalysts at atmospheric pressure (6a). For the present catalyst, the observed 2-mp/3-mp mole ratio is 10–15% in excess of the equilibrium ratio of 2.0 at 300°C. Formation of 2,3-dmb is not kinetically favorable, as it requires two carbenium ion skeletal isomerization steps and consequently a longer lifetime for the carbocation intermediate. Among the light alkane products, the large yields of propane, isobutane, and isopentane are diagnostic of hydrocracking, which is consistent with the bifunctional nature of the catalyst (18). Metal-catalyzed hydrogenolysis occurs, but the $C_1/\Sigma C_5$ and $C_2/\Sigma C_4$ molar ratios are 0.17 and 0.15, respectively, indicating that these reactions account for about 15% or less of the cracking yield. The formation of C_4 and C_5 alkanes can be explained by acid-catalyzed oligomerization of hexenes and subsequent hydrocracking (6a). We infer that mcp is produced by monofunctional Pt catalysis.

Arrhenius behavior was observed for the formation of the C_6 branched alkane isomers, C_3–C_5 cracking products, and mcp (Fig. 1) in the range of 240 to 300°C. In contrast, the apparent activation energies for the formation of methane and ethane increased with increasing temperature, suggesting a change in the reaction mechanism with temperature. The apparent activation energies for the individual isomerization products are nearly equal (Table 3), which is consistent with their formation by a common mechanistic pathway. The situation is similar for the C_3–C_5 cracking products; the average activation energy (37 kcal/mol) agrees well with the activation energy reported for *n*-hexane cracking by Pt–H–Y catalysts (35 kcal/mol) (19). The activation energy for dehydrocyclization of *n*-hexane to mcp is also in reasonable agreement with literature values for Pt–zeolite catalysts (39 kcal/mol) (20).

In contrast, the observed activation energy for *n*-hexane isomerization over Pt–H–MOR is approximately one-half of the average of values reported for this reaction over similar metal–zeolite bifunctional catalysts: Pt–H–MOR (29–36 kcal/mol) (6, 21, 22), Pt–H–Y (37 kcal/mol) (19), and Pd–H–MOR (34 kcal/mol) (23). Because the activa-

TABLE 3

Apparent Activation Energies for Isomerization and Cracking of *n*-hexane over Pt–MOR Catalysts

Product	Catalyst	
	Pt–H–MOR	Pt–KH–MOR
	E_a (kcal/mol)	
Methane	[a]	25
Ethane	[a]	[a]
Propane	40	23
Isobutane	37	[b]
n-butane	35	23
Isopentane	37	[b]
n-pentane	35	21
2,3-dmb	16	[b]
2-mp	14	44
3-mp	15	43
mcp	32	32

[a] Non-Arrhenius behavior: E_a appeared to increase with increasing temperature.

[b] Rate of formation was too low to allow an accurate determination of the apparent activation energy.

tion energy for isomerization is lower than that for hydrocracking, isomerization selectivity is higher at lower temperatures. The unusually low apparent activation energies of the isomerization products suggest that the true values may be disguised by pore diffusion effects. Isomerization proceeds at the highest rates and may approach equilibrium within the pores, if transport of reactants and/or products is diffusionally limited. According to the continuum Thiele reaction–diffusion model, in the limit of strong pore-diffusion limitations the effectiveness factor (η) is inversely proportional to the Thiele modulus (ϕ). For a first-order reversible reaction, the Thiele modulus contains the reaction equilibrium constant (K_{eq}) in addition to the forward rate constant, the effective diffusion coefficient (D_e), and the diffusion length (24). Under conditions of strong pore diffusional limitations (i.e., $\eta \propto 1/\phi$), it can be shown that the observed activation energy will be

$$E_{obs} = \tfrac{1}{2}\left[E_a + E_d + \frac{\Delta H_{rxn}}{(1 + K_{eq})}\right],$$

where E_a is the true apparent activation energy, E_d is the activation energy for diffusion, and ΔH_{rxn} is the reaction enthalpy change. For the conversion of *n*-hexane to 2-mp at 300°C, K_{eq} is approximately 1.8, and ΔH_{rxn} is approximately −2 kcal/mol. Thus, E_{obs} will be approximately one-half of E_a, which is consistent with the results obtained for *n*-hexane isomerization over Pt–H–MOR. Moreover, Guisnet *et al.* (6a) have reported that for Pt–H–MOR catalysts with a Si/Al ratio of 8, the maximum rate of *n*-hexane isomerization at atmospheric pressure and 250°C was observed for catalysts containing 0.3 wt% Pt. The decrease in the rate for catalysts with higher Pt loadings was attributed to partial blockage of the mordenite channels by Pt crystallites. The characterization results (*vide infra*) suggest that the present Pt–H–MOR catalyst contains Pt clusters hosted within the mordenite crystals which could restrict the diffusion of C_6 molecules within the unidirectional channels.

Pt–KH–MOR Catalysts. The elemental composition of the Pt–KH–MOR catalyst is given in Table 1. Assuming complete reduction of Pt, this corresponds to a unit cell formula of $H_{0.5}K_{4.1}Al_{4.6}Si_{43.4}O_{96}$, which is consistent with the reported Si/Al ratio of 9.2 and indicates approximately 90% exchange of protons for K^+. As expected, the Pt loading was nearly equal to that of the Pt–H–MOR catalyst prior to exchange. Pt–KH–MOR catalysts were tested for *n*-hexane conversion following *in situ* reduction in flowing H_2 at 350°C.

The catalytic activity of Pt–KH–MOR for *n*-hexane conversion was lower than that of Pt–H–MOR, but the isomerization selectivity was higher. In addition, benzene was formed over Pt–KH–MOR with an estimated yield

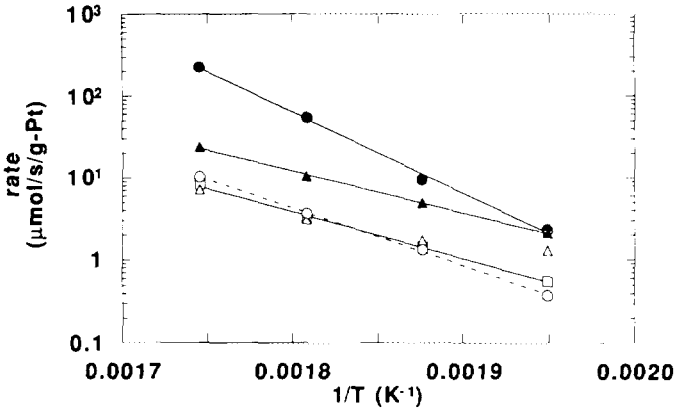

FIG. 2. Arrhenius plot for *n*-hexane conversion over Pt–KH–MOR: $\Sigma(i\text{-}C_6)$ (solid circles), $\Sigma(C_1\text{-}C_3)$ (solid triangles), ethane (open triangles), methane (open squares), methylcyclopentane (open circles). Reaction conditions: P = 1 atm, H_2: HC = 4.0 (molar basis).

of less than 1% at 300°C and 1 atm (H_2: HC = 4). The branched-isomer yield at 300°C was nearly 90% (Table 2), owing chiefly to strong suppression of hydrocracking activity. In comparison to the Pt–H–MOR catalyst, the yield of propane was reduced by a factor of more than 4, and the yields of isobutane and isopentane were reduced by a factor of more than 10. We infer that sufficient acid sites remained after K^+ exchange to allow *n*-hexane isomerization via bifunctional catalysis, because catalysts which were subjected to more extensive K^+ exchange exhibited very low activity and low isomerization selectivity. In fact, *n*-hexane isomerization over Pt–KH–MOR may be a better example of bifunctional catalysis than this reaction over Pt–H–MOR, because the metal and acid functions are in better balance. The strong suppression of hydrocracking activity by partial K^+ exchange indicates that hydrocracking requires a higher density of strong acid sites than bifunctional isomerization. Moreover, *n*-hexane isomerization to 2,3-dmb was suppressed, which is consistent with a shorter carbocation lifetime.

Arrhenius behavior was observed for the formation of C_6 branched isomers, C_3–C_5 hydrocarbons, mcp, and methane over Pt–KH–MOR in the range of 240 to 300°C (Fig. 2). The ethane formation rate was anomalously high at 240°C, but at higher temperatures, the apparent activation energy is similar to that of methane formation. In contrast to the behavior of Pt–H–MOR, the isomerization selectivity of Pt–KH–MOR increased substantially with increasing temperature, as the apparent activation energies for formation of light alkanes and mcp are substantially lower than for isomerization (Table 3). The apparent activation energy for isomerization over Pt–KH–MOR is more than double that observed for Pt–H–MOR and is in reasonable agreement with values reported for metal–hydrogen–zeolite catalysts. This result supports

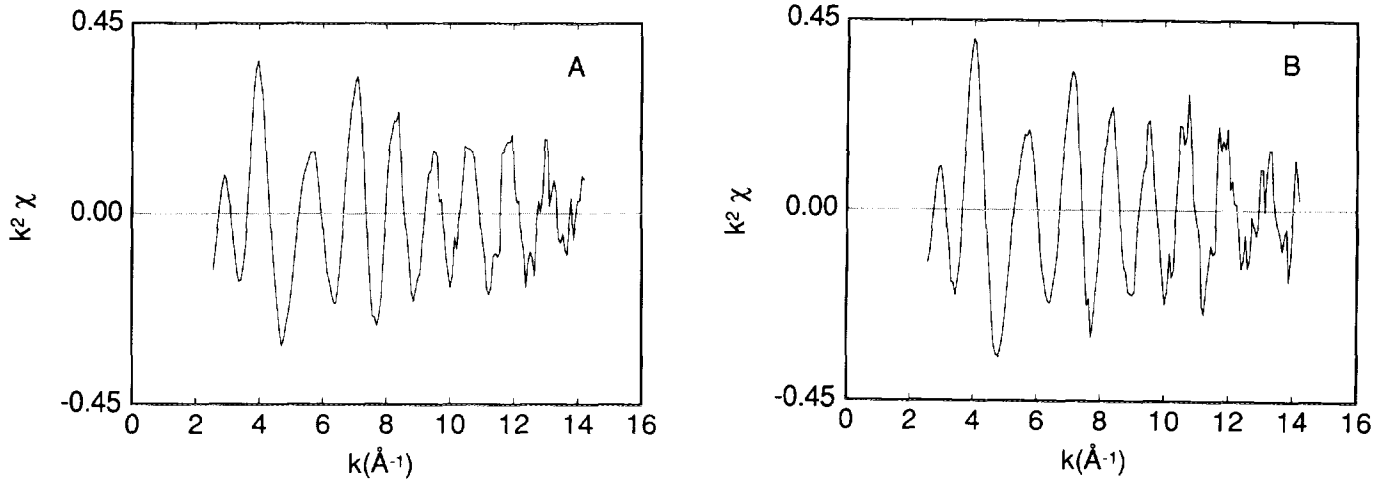

FIG. 3. Pt L_{III} EXAFS spectra of (A) Pt–H–MOR and (B) Pt–KH–MOR.

the hypothesis that in Pt–H–MOR most of the acid sites were ineffective for isomerization owing to diffusional limitations. Even after 90% of the acid sites were poisoned, the isomerization activity of Pt–KH–MOR was less than a factor of 2 lower than that of Pt–H–MOR at 300°C. In contrast, the Pt–H–MOR catalyst was a factor of 30 more active at 240°C.

The low yields of branched isomers and the distribution of C_1–C_5 products over Pt–KH–MOR suggest that light alkanes are formed primarily by hydrogenolysis of *n*-hexane. In contrast to Pt–H–MOR, the $C_1/\Sigma C_5$ and $C_2/\Sigma C_4$ molar ratios are close to 1.0, as expected for *n*-hexane hydrogenolysis. The apparent activation energies determined for formation of methane, propane, *n*-butane, and *n*-pentane (Table 3) agree well with reported activation energies for alkane hydrogenolysis (e.g., 28 kcal/mol for *n*-pentane hydrogenolysis over Pt/SiO_2 (25), and 22–26 kcal/mol for *n*-hexane over single-crystal Pt(26)). The apparent activation energy for mcp formation was unaffected by K^+ exchange; the increased rate is inferred to result from an increase in the active site density for this Pt-catalyzed reaction.

2. *Catalyst Characterization*

EXAFS spectroscopy. The Pt–H–MOR and Pt–KH–MOR catalysts were characterized by *in situ* X-ray absorption spectroscopy following reduction in flowing H_2 at 350°C for 1 h. The Pt L_{III} EXAFS spectra (Fig. 3) are closely similar and are characteristic of highly dispersed Pt. These qualitative conclusions were confirmed by analysis of the Fourier-filtered first-shell data. The k^2-weighted spectrum of the Pt–H–MOR catalyst (Fig. 3A) was Fourier transformed ($2.8 < k < 13.3$ Å^{-1}), and the resultant radial structure function was inverse transformed ($1.28 < R < 3.18$ Å) to isolate the first coordination shell. Using the first shell of Pt foil as a reference, the Pt–Pt contribution was estimated by fitting the inverse transform (Fig. 4A) in k space between 6.0 and 12.8 Å^{-1}. The result is given in Table 4. Within the fitting range, there is good agreement between the calculated Pt–Pt contribution and the first-shell data in k space and R space, as illustrated in Figs. 4A and 4C. The large deviations at low energies ($k < 7$ Å^{-1}) are due to backscattering from low-Z elements (27, 28). A detailed analysis of these contributions, which we believe are associated with the Pt–zeolite interface, will be presented elsewhere.

The EXAFS spectrum of the Pt–KH–MOR catalyst (Fig. 3B) was analyzed similarly. The forward and inverse transform ranges were $2.8 < k < 12.9$ Å^{-1} and $1.22 < R < 3.18$ Å, respectively, and the inverse transform was fitted in k space between 6.0 and 12.4 Å^{-1}. The result is given in Table 4, and the calculated Pt–Pt contribution is compared with the Fourier-filtered data in Figs. 4B and 4D. Significantly, the first-shell Pt–Pt coordination parameters obtained from EXAFS spectroscopy are equivalent within experimental uncertainty for the Pt–H–MOR and Pt–KH–MOR catalysts.

If Pt–Pt bonding (metal atom connectivity) is maximized in the clusters, the observed Pt–Pt coordination numbers indicate an average cluster nuclearity of about six atoms. Moreover, the average Pt–Pt bond distance is shorter than bulk value by 0.05 Å, even though the clusters are saturated by adsorbed hydrogen. This result is consistent with small, electron-deficient Pt clusters. By approximating the cluster shape as octahedral, we estimate an average cluster size of 6.6 Å, just small enough to fit within the mordenite channels. These observations suggest that the Pt clusters are intracrystalline and that their size is nearly unique, as it is limited in two dimensions by the

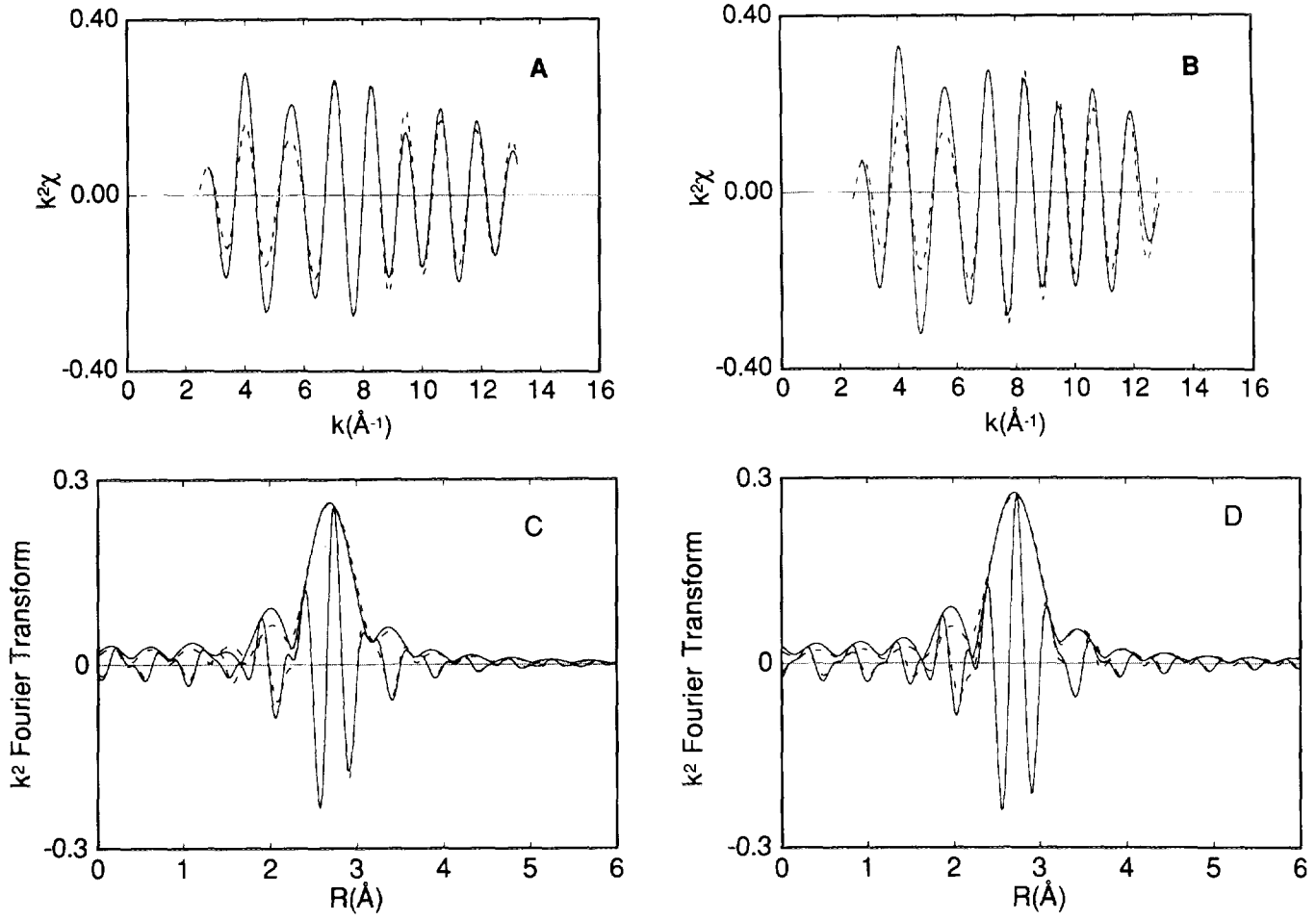

FIG. 4. Comparison of k^2-weighted first-shell EXAFS data (solid curves) and calculated best fits (dashed curves) in k and R space: (A) Pt-H-MOR chi functions and (B) Pt-KH-MOR chi functions; (C) Pt-Pt phase-corrected Fourier transforms ($6.0 < k < 12.8$ Å^{-1}) associated with A and (D) Pt-Pt phase-corrected Fourier transforms ($6.0 < k < 12.4$ Å^{-1}) associated with B.

mordenite channels. We infer that the low Pt loading, which is equivalent to only 1 atom/120 Å of pore length, limited cluster growth along the channel direction. Similar results have been reported by Koningsberger and coworkers (29) for Pt clusters in BaK-L zeolite, which like mordenite has a unidirectional channel structure. Apparently, the clusters are well-anchored within the pores as the cluster size is unaffected by K^+ exchange and rereduction.

TABLE 4

Pt-Pt Contributions to the EXAFS Spectra of Pt-MOR Catalysts

Catalyst	N[a]	R[b] (Å)	$\Delta\sigma^2$ (Å^2)	ΔE_0 (eV)
Pt-H-MOR	3.7	2.72	0.0058	3.1
Pt-KH-MOR	3.9	2.72	0.0055	1.3

[a] Pt-Pt coordination number; estimated uncertainty: ±15%.
[b] Pt-Pt nearest neighbor distance; estimated uncertainty: ±0.01 Å.

The EXAFS spectra of a freshly reduced Pt-H-MOR catalyst and the same sample after catalysis of *n*-hexane isomerization at 300°C and 1 atm (4 : 1 H_2 : HC) for 1 h are compared in Figure 5. The high-k data evidence that the Pt morphology was essentially unchanged after catalysis, indicating that the clusters were stable under the reaction conditions, at least in the short term. In addition, because the EXAFS amplitudes are closely similar at low energy ($k < 8$ Å^{-1}), we infer that the cluster surfaces remained relatively free of covalently bonded hydrocarbon moieties during catalysis.

H_2 TPD. The H_2 temperature-programmed desorption spectrum of a freshly reduced Pt-H-MOR catalyst contains peaks at 115, 220, 350, and 550°C. The spectrum (Fig. 6A) is in good agreement with that reported by Lerner *et*

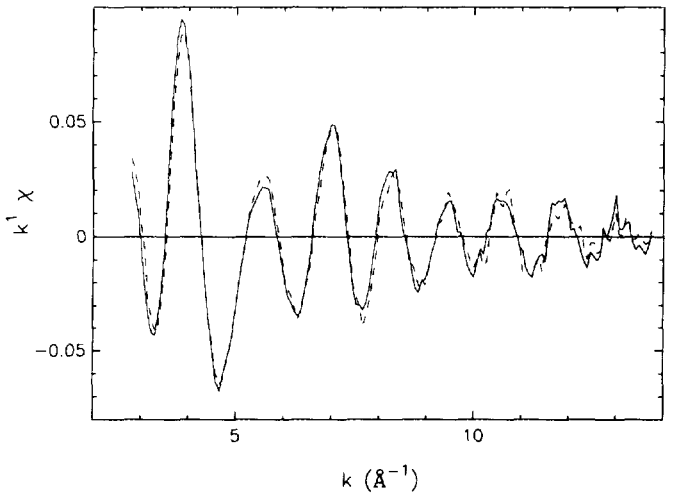

FIG. 5. *In situ* EXAFS spectra of freshly reduced Pt–H–MOR (solid curve) and the catalyst after *n*-hexane conversion (H_2 : HC = 4) at 300°C and 1 atm for 1 h on-stream time (dashed curve).

al. for a 0.49% Pt–H–MOR catalyst reduced at 350°C in H_2 (30). The sharp, low-temperature peak (designated by α) is assigned to desorption of H_2 from Pt clusters, in agreement with the previous work. The H/Pt ratio associated with the α peak $(H/Pt)_\alpha$ and the total H/Pt value for the spectrum are given in Table 5. The values are indicative of highly dispersed Pt and are in good agreement with those reported by Sachtler and co-workers for a 1% Pt–H–MOR catalyst which was reduced at 350°C in H_2 (30). The assignment of the high-temperature desorption peaks is more ambiguous, since it is unlikely that H_2 adsorbed on Pt clusters would require temperatures greater than 300°C for desorption. Sachtler and co-workers proposed that these peaks arise from oxidation of

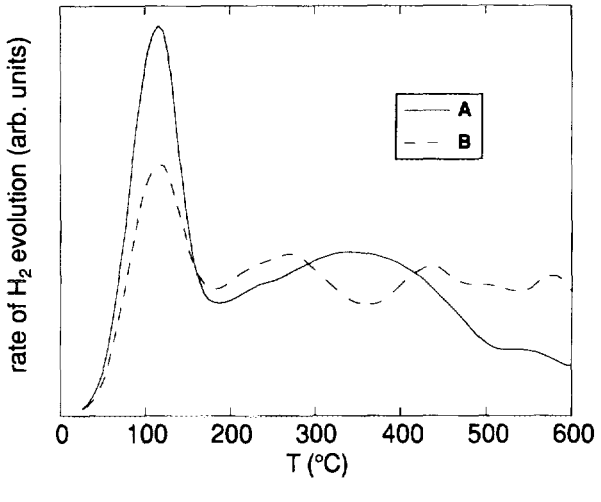

FIG. 6. H_2 TPD spectra of (A) Pt–H–MOR and (B) Pt–KH–MOR.

TABLE 5

H/Pt Ratios of Pt–MOR Catalysts Determined by H_2 TPD

Catalyst	$(H/Pt)_\alpha$[a]	$(H/Pt)_{total}$[b]
Pt–H–MOR	0.85	2.47
Pt–KH–MOR	0.65	2.49

[a] Integration range: 25 to 180°C.
[b] Integration range: 25 to 600°C.

isolated Pt atoms by zeolite protons (30). We favor an alternative interpretation, because extensive K^+ back exchange to remove protons shifted but did not significantly reduce the intensity of the high-temperature desorption peaks (*vide infra*). We infer that the broad desorption features at 350 and 550°C in the H_2 TPD spectrum of Pt–H–MOR arise from desorption of spilled-over H_2. This interpretation is supported by the recent work of Koningsberger and co-workers which examined H_2TPD from Pt–L zeolite, Pt–Omega, and Pt/Al_2O_3 catalysts (31).

The H_2 TPD spectrum (Fig. 6B) of Pt-KH-MOR contains peaks at 115, 215, 275, 430, 500, and 580°C. In comparison to the spectrum of Pt–H–MOR, the α peak area is reduced by about 25%, but the total H/Pt ratio is nearly the same (Table 4). For Pt–KH–MOR there is an increase in H_2 desorption between 200 and 300°C relative to that observed for Pt–H–MOR. As the EXAFS analysis indicates that the Pt cluster size was not affected by K^+ exchange, we infer the (H/Pt) ratio for chemisorption should be approximately the same in the two catalysts. Consequently, we suggest that the peaks at 215 and 275°C in the H_2 TPD spectrum of Pt/KH–MOR arise from desorption of more strongly chemisorbed H_2. The amount of H_2 desorbed at temperatures greater than 300°C is relatively unchanged by K^+ exchange, but the peaks are shifted to higher temperatures. This is indicative of a change in the nature of the spilled-over H species owing to K^+ modification of the mordenite.

XANES spectroscopy. Analysis of the X-ray absorption near-edge structure spectra of the catalysts revealed that the acid–base character of the mordenite had no detectable effect on the electronic structure of the Pt clusters. In Fig. 7, the XANES spectra of the freshly reduced catalysts are compared to that of a Pt foil reference which was measured simultaneously. For each catalyst, an apparent edge shift (ΔE) of about 1 eV toward higher binding energy is observed (Table 6). Similar Pt L_{III} edge shifts were reported for highly dispersed Pt/SiO_2 and Pt/Al_2O_3 catalysts (32); these data were interpreted as indicating that the supported Pt clusters were electron deficient relative to the bulk metal. We caution that the apparent edge

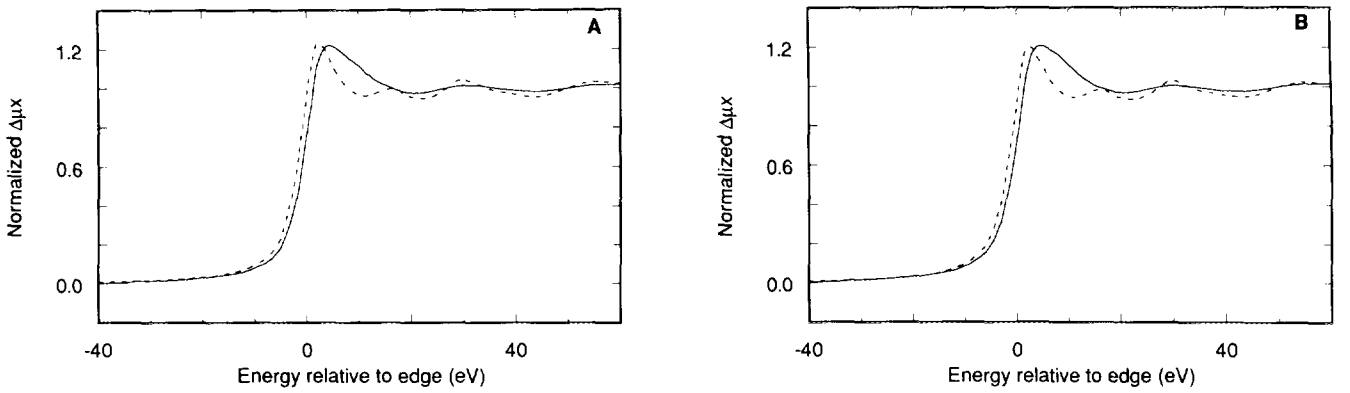

FIG. 7. Normalized Pt L_{III} XANES spectra of the freshly reduced catalysts (solid curves) and a Pt foil reference (dashed curve): (A) Pt–H–MOR and (B) Pt–KH–MOR.

shifts could result from changes in the L_{III} threshold resonance rather than shifts of the continuum absorption threshold.

In Fig. 7, it is apparent that the L_{III} threshold resonance (white line) of the Pt clusters is altered in shape and area in comparison to that of Pt foil. The L_{III} resonance is due to electronic transitions from $2p_{3/2}$ states to unoccupied $5d$ bound states; its intensity correlates with the number of d band holes (33). For bulk Pt, a sharp Lorentzian peak centered at about 4 eV relative to the L_{III} edge is observed, and the maximum corresponds to the Fermi level (E_F) (34). The effects of cluster size and adsorbed H_2 on Pt electronic structure are best illustrated in the difference spectra (Fig. 8), which were created by subtraction of the normalized spectrum of Pt foil from the normalized and edge-shift-corrected spectra of the catalysts. For the Pt–H–MOR and Pt–KH–MOR catalysts, the difference spectra (Fig. 8A) are closely similar, indicating that the nature of the charge-compensating cation has little effect on the electronic structure of the hosted Pt clusters. This result is consistent with the earlier work which found no detectable differences in the Pt L_{III} XANES spectra of a series of Pt–*M*–Y (*M* = H, Na, and Ce catalysts (16).

In agreement with XANES difference spectra reported by others (16, 35) for highly dispersed supported Pt, two principal features are observed in the region between −10 and 20 eV: a small negative peak at 4 eV and a broad positive peak at 11 eV. The feature at 11 eV is associated chiefly with H_2 adsorption by the Pt clusters, as its intensity is reduced significantly by evacuation of Pt–H–MOR at 300°C (Fig. 8b). Concomitantly, there is a shift of the apparent absorption threshold by approximately 0.5 eV toward lower energy. Samant and Boudart (16) suggested that this XANES feature is due to electronic transitions from Pt $2p_{3/2}$ states to unoccupied Pt–H antibonding states. This is reasonable as H_2 chemisorption on Pt is expected to create occupied Pt–H bonding states below E_F and unoccupied antibonding states above E_F (36). After accounting for the influence of chemisorbed H_2 on the XANES spectra, we infer that the negative difference at 4 eV and the residual positive difference at 11 eV result from broadening and shifting of the L_{III} threshold resonance toward higher energies. This could arise from quantum size effects on Pt electronic structure and/or from cluster–host interactions. After H_2 desorption, the net area difference between −10 and 17 eV is small, indicating that there is little change in the number of d band holes relative to bulk Pt.

TABLE 6

L_{III} Edge Shifts of Pt–MOR Catalysts Relative to Pt foil

Catalyst	Description	ΔE (eV)[a]
Pt–H–MOR	H_2-covered Pt	1.2
	Evacuation at 300°C	0.7
Pt–KH–MOR	H_2-covered Pt	1.2

[a] The estimated experimental uncertainty is ±0.5 eV.

CO adsorption. Notwithstanding the absence of an electronic effect on the hosted Pt clusters, the acid–base character of the mordenite did have a significant influence on the infrared spectrum of adsorbed CO. The infrared spectra of CO adsorbed on Pt–H–MOR are shown in Fig. 9A. At saturation coverage, bands are observed at 2124, 2084, and 1870 cm^{-1}. The position of the intense linear ν_{CO} band shifts toward lower wavenumbers as CO coverage is reduced by *in vacuo* desorption. This effect arises from a reduction of dipole–dipole interactions between neighboring CO moieties in the adsorbed layer as coverage decreases (37). Extrapolation to zero coverage gives an

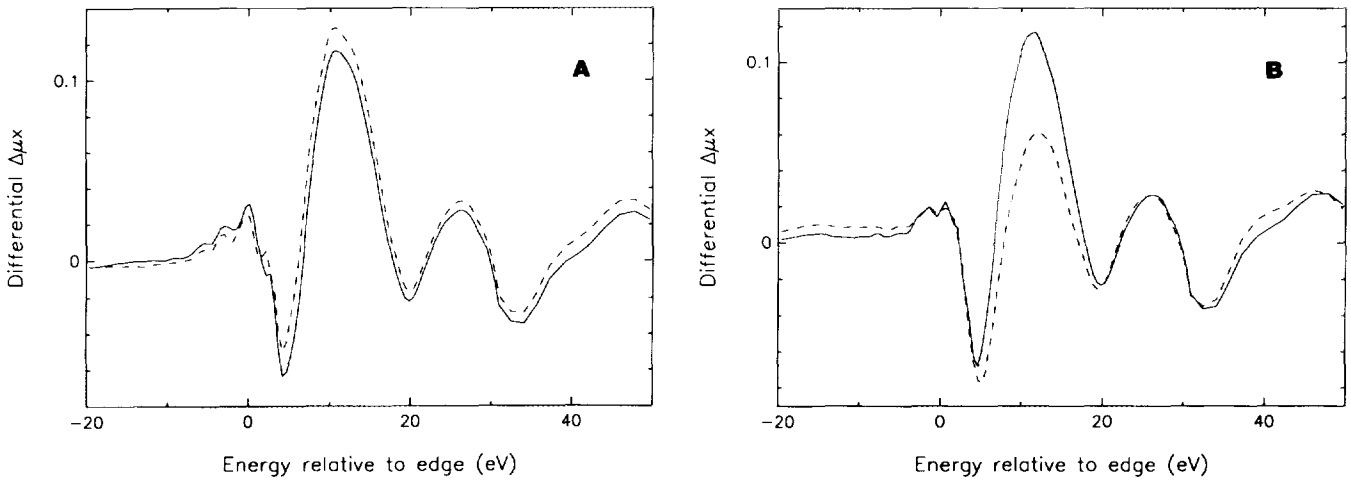

FIG. 8. XANES difference spectra of (A) freshly reduced Pt–KH–MOR (solid curve) and freshly reduced Pt–H–MOR (dashed curve); (B) freshly reduced Pt–H–MOR (solid curve) and sample after evacuation at 300°C for 0.5 h (dashed curve).

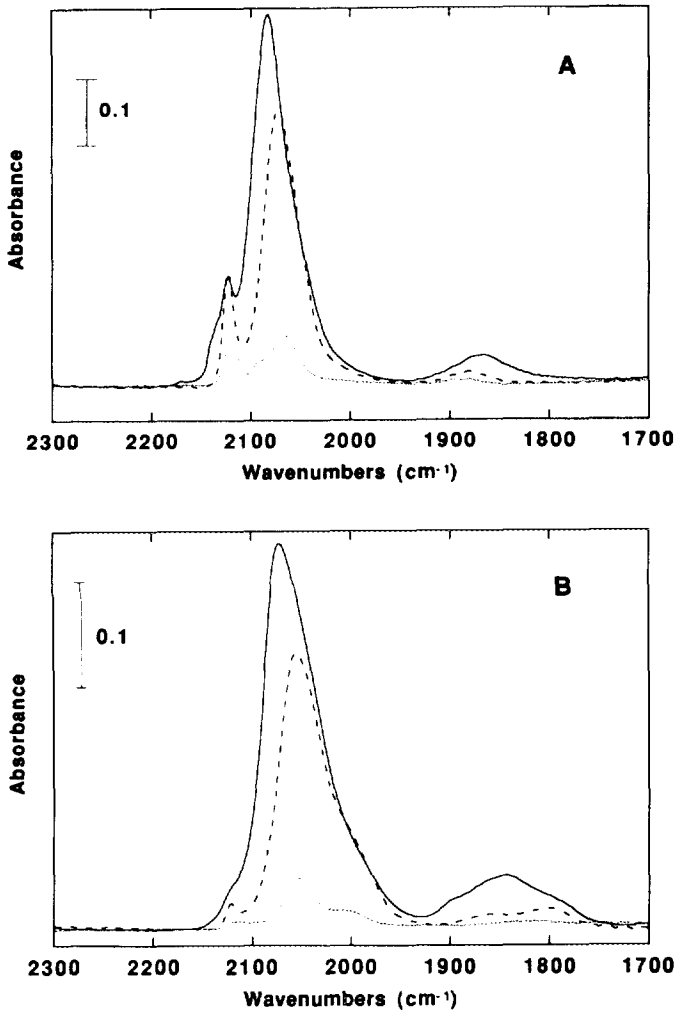

FIG. 9. Infrared spectra of (A) Pt–H–MOR and (B) Pt–KH–MOR after exposure to 100 Torr CO and evacuation at 30°C (solid curves), 100°C (dashed curves), and 200°C (dotted curves).

estimated ν_{CO} frequency of approximately 2065 cm^{-1} for isolated linear CO moieties on the Pt clusters. The 1870-cm^{-1} bridging ν_{CO} band appears to shift slightly to higher wavenumbers with decreasing coverage. This could be explained if the bridging CO band consisted of two peaks due to species of different thermal stabilities. If the lower wavenumber peak were associated with the less stable species, the apparent shift could be explained.

The species responsible for the 2124-cm^{-1} peak has a higher thermal stability than linear and bridged CO moieties on the Pt clusters, as this peak is unaffected by CO desorption at 100°C *in vacuo* (Fig. 9A). The absence of dipolar interactions, as evidenced by the sharpness of the band and invariance of the peak position with CO coverage, indicates that this species is associated with isolated Pt centers. The location of the peak suggests that this Pt species is in a low positive oxidation state. Kustov and Sachtler (38) assigned this peak to CO adsorbed on very small clusters or monoatomic Pt^{I} monocarbonyl species; we favor the latter assignment. A Pt^{I}–CO species might be formed by CO adsorption on small Pt clusters which are hosted in the strongly acidic mordenite matrix. A similar oxidative fragmentation of Rh clusters supported on γ-Al_2O_3 occurs concomitant with CO adsorption at 25°C (39). EXAFS spectra of Pt–H–M measured after exposure to CO, while not of sufficient quality to justify a complete analysis, are suggestive of cluster fragmentation. Moreover, a substantial increase of the Pt L_{III} white line area was induced by CO adsorption.

The infrared spectra of adsorbed CO on Pt–KH–MOR are shown in Fig. 9B. At saturation coverage, bands are observed at 2120 (sh), 2073, 1990 (sh), 1895 (sh), 1845, and 1795 (sh) cm^{-1}. In comparison to the spectrum of CO adsorbed on Pt–H–MOR, the linear ν_{CO} band is broad-

ened and red-shifted by approximately 10 cm^{-1} and the bridging CO bands are substantially more intense. The location of the linear CO band is coverage dependent; extrapolation of the ν_{CO} frequency to zero coverage gives 2050 cm^{-1}, which is 15 cm^{-1} less than the corresponding frequency for Pt–H–MOR. For Pt–zeolite catalysts, a red shift of the linear ν_{CO} band is usually observed as the support is made more basic (16, 40). These shifts have been interpreted in terms of changes in Pt *d* electron occupancy, which in turn affect d–π^* back-bonding with CO. Using this model, the observed red shift would be indicative of greater Pt *d* electron density (fewer *d* holes) for Pt–KH–MOR than for Pt–H–MOR. Conversely, the Pt clusters in Pt–H–MOR would appear to be more electron deficient. However, the XANES results indicate that the *d* electron occupancy and core levels of Pt atoms in the clusters are unaffected by exchange of H^+ by K^+. Consequently, we sought an alternative explanation for the effect of K^+ exchange on the infrared spectrum of adsorbed CO.

Changes in the electrostatic environment within the mordenite channels following K^+ exchange could directly affect the adsorbed CO molecules. In Na–MOR, the cations are located primarily in the side pockets along the main channels (41). If K^+ ions were placed in these sites by exchange, they could interact with the basic O atoms of adsorbed carbonyl moieties. C- and O-bonded carbon monoxide ligands are more π-acidic than terminally bonded ligands and are characterized by lower ν_{CO} frequencies (42). Interaction of the K^+ ions with carbonyl O atoms could also explain the observed increase in the proportion of bridging CO moieties following K^+ exchange. For Pt–KH–MOR, the ratio of bridging to linear ν_{CO} band areas is 0.15, twice that observed for Pt–H–MOR. The O atoms of bridging CO moieties are expected to interact more strongly with K^+ ions. In molecular metal carbonyl clusters, the O atoms of bridging CO ligands are more basic than those of terminally bonded CO ligands. Bridging carbonyls are the preferred sites of cation attachment in anionic metal carbonyl clusters, and CO ligands are known to switch from terminal to bridged configurations in order to interact more favorably with metal cations and molecular Lewis acids (42).

The 2120-cm^{-1} peak which was assigned to isolated Pt^1 sites is much weaker in Fig. 9B than in Fig. 9A. This is consistent with the previously suggested role of mordenite protons in the oxidative fragmentation of small Pt clusters. Among the other bands observed in Fig. 9B, the peaks at 1990 and 1795 cm^{-1} are suggestive of molecular Pt carbonyl clusters, in particular the Chini-Longoni $[Pt_3(CO)_6]_n^{2-}$ clusters (43). For example, the hexaplatinum cluster (n = 2) exhibits ν_{CO} bands at 1995, 1818, and 1795 cm^{-1}. As basic conditions are required for the syntheses of these clusters in solution, K^+ exchange of Pt–MOR should favor their formation. Moreover, syntheses of anionic Pt carbonyl clusters in the supercages of basic alkali-exchanged faujasites (44) and on the surface of basic MgO (45) have been reported. We suggest that these clusters are formed as minority species by CO adsorption on Pt–KH–MOR; higher yields should be possible by reductive carbonylation of Pt(II)–K–MOR with CO or CO + H_2 mixtures.

ACKNOWLEDGMENTS

The authors thank Professor G. W. Roberts for fruitful discussions regarding the reaction-diffusion problem, and Professor D. E. Sayers for his help with the EXAFS analysis. This research was supported by an NSF Presidential Young Investigator Award (CTS-8958350) and matching contributions from Mobil Research and Development Corporation. X-ray absorption spectrascopy research was carried out at the National Synchrotron Light Source, Brookhaven National Laboratory. We thank the staff of beamline X-11 for their assistance.

REFERENCES

1. Bernard, J. R., *in* "Proceedings of 5th International Conference of Zeolites" (L. V. C. Rees, Ed.), p. 686. Heyden, London, 1980.
2. Tauster, S. J., and Steger, J. J., *J. Catal.* **125,** 387 (1990).
3. Vaarkamp, M., Miller, J. T., Modica, F. S., Lane, G. S., and Koningsberger, D. C., *J. Catal.* **138,** 675 (1992).
4. Mielczarski, E., Hong, S. B., David, R. J., and Davis, M. E., *J. Catal.* **134,** 359 (1992).
5. Kouwenhoven, H. W., *ACS Adv. Chem. Ser.* **121,** 529 (1973).
6. (a) Guisnet, M., Fouche, V., Belloum, M., Bournonville, J. P., and Travers, C., *Appl. Catal.* **71,** 283 (1991); (b) Guisnet, M., Fouche, V., Belloum, M., Bournonville, J. P., and Travers, C., *Appl. Catal.* **71,** 295 (1991).
7. Ribeiro, F. R., *in* "Zeolites: Science and Technology" (F. R. Ribeiro, A. E. Rodrigues, L. D. Rollman, and C. Naccache, Eds.), p. 545. Nijhoff, The Hague, 1984.
8. Guisnet, M., and Perot, G., *in* "Zeolites: Science and Technology" (F. R. Ribeiro, A. E. Rodrigues, L. D. Rollman, and C. Naccache, Eds.), p. 397. Nijhoff, The Hague, 1984.
9. Dalla Betta, R. A., and Boudart, M., *in* "Proceedings of the 5th International Congress on Catalysis," Vol. 2, p. 1329. North-Holland, New York, 1972.
10. Dessau, R. M., *J. Catal.* **89,** 520 (1984).
11. Gallezot, P., *Catal. Rev. Sci. Eng.* **20,** 121 (1979).
12. Vedrine, J. C., Dufaux, M., Naccache, C., and Imelik, B., *J. Chem. Soc. Faraday Trans.* **74,** 440 (1978).
13. Foger, K., and Anderson, J. R., *J. Catal.* **54,** 318 (1978).
14. Naccache, C., Primet, M., and Mathieu, M. V., *ACS Adv. Chem. Ser.* **121,** 66 (1973).
15. Gallezot, P., Weber, R., Dalla Betta, R. A., and Boudart, M., *Z. Naturforsch. A* **34,** 40 (1979).
16. Samant, M. G., and Boudart, M., *J. Phys. Chem.* **95,** 4070 (1991).
17. Sayers, D. E., and Bunker, B. A., *in* "X-Ray Absorption: Principles, Applications, Techniques of EXAFS, SEXAFS, and XANES," (D. C. Koningsberger and R. Prins, Eds.), p. 211. Wiley, New York, 1988
18. Gates, B. C., "Catalytic Chemistry." Wiley, New York, 1992.
19. (a) Ribeiro, F., Marcilly, C., and Guisnet, M., *J. Catal.* **78,** 267 (1982); (b) Ribeiro, F., Marcilly, C., and Guisnet, M., *J. Catal.* **78,** 275 (1982).

20. Lane, G. S., Modica, F. S., and Miller, J. T., *J. Catal.* **129,** 145 (1991).
21. Spivey, J. J., and Bryant, P. A., *Ind. Eng. Chem. Process Res. Dev.* **21,** 750 (1982).
22. Braun, G., Fetting, F., and Schoeneberger, H., *ACS Symp. Ser.* **40,** 504 (1977).
23. Chick, D. J., Katzer, J. R., and Gates, B. C., *ACS Symp Ser.* **40,** 515 (1977).
24. Satterfield, C. N., "Mass Transfer in Heterogeneous Catalysis," p. 194. MIT Press, Cambridge, MA, 1970.
25. Kikuchi, E., Tsurumi, M., and Morita, Y., *J. Catal.* **22,** 226 (1971).
26. Davis, S. M., Zaera, F., and Somorjai, G. A., *J. Catal.* **85,** 206 (1984).
27. Koningsberger, D. C., and Sayers, D. E., *Solid State Ionics* **16,** 23 (1981).
28. Kip, B. J., Duivenvoorden, F. B. M., Koningsberger, D. C., and Prins, R., *J. Catal.* **105,** 26 (1987).
29. Vaarkamp, M., Grondelle, J. V., Miller, J. T., Sajkowski, D. J., Modica, F. S., Lane, G. S., Gates, B. C., and Koningsberger, D. C., *Catal. Lett.* **6,** 369 (1990).
30. Lerner, B. A., Carvill, B. T., and Sachtler, W. M. H., *J. Mol. Catal.* **77,** 99 (1992).
31. Vaarkamp, M., Ph.D. dissertation, University of Utrecht, The Netherlands, 1993.
32. Mansour, A. N., Cook, J. W., Jr., Sayers, D. E., Emrich, R. J., and Katzer, J. R., *J. Catal.* **89,** 462 (1984).
33. Lytle, F. W., *J. Catal.* **43,** 376 (1976).
34. Bianconi, A., *in* "X-Ray Absorption: Principles, Applications, Techniques of EXAFS, SEXAFS, and XANES" (D. C. Koningsberger and R. Prins, Eds.), p. 573. Wiley, New York, 1988.
35. Meitzner, G., Via, G. H., Lytle, F. W., and Sinfelt, J. H., *J. Phys. Chem.* **96,** 4960 (1992).
36. Saillard, J.-Y., and Hoffman, R., *J. Am. Chem. Soc.* **106,** 2006 (1984).
37. Eischens, R. P., and Pliskin, W. A., *Adv. Catal.* **10,** 1 (1958).
38. Kustov, L. M., and Sachtler, W. M. H., *J. Mol. Catal.* **71,** 233 (1992).
39. van't Blik, H. F. J., van Zon, J. B. A. D., Huizinga, T., Vis, J. C., Koningsberger, D. C., and Prins, R., *J. Am. Chem. Soc.* **107,** 3139 (1985).
40. Besoukhanova, C., Guidot, J., Barthomeuf, D., Brevsse, M., Bernard, J. R., *J. Chem. Soc., Faraday Trans. 1* **77,** 1595 (1981).
41. Barrer, R. M., and Peterson, D. L., *Proc. R. Soc. A* **280,** 466 (1964).
42. Horwitz, C. P., and Shriver, D. F., *Adv. Organometal. Chem.* **23,** 219 (1984).
43. Longoni, G., and Chini, P., *J. Am. Chem. Soc.* **98,** 7225 (1976).
44. Puga, J., Patrini, R., Sanchez, K. M., and Gates, B. C., *Inorg. Chem.* **30,** 2479 (1991).
45. Chang, J.-R., Koningsberger, D. C., and Gates, B. C., *J. Am. Chem. Soc.* **114,** 6460 (1992).